International Journal of Automotive Technology, Vol. 15, No. 2, pp. 219–227 (2014)
DOI 10.1007/s12239–014–0023–9

pISSN 1229–9138/ eISSN 1976–3832

REVIEW ON CHARACTERIZATION OF NANO-PARTICLE EMISSIONS AND PM MORPHOLOGY FROM INTERNAL COMBUSTION ENGINES: PART 2

S. CHOI[1)], C. L. MYUNG[2)*] and S. PARK[2)]

[1)]Transportation Technology R&D Center, Energy System Division, Argonne National Laboratory, 9700 South Cass Avenue, Argonne, IL 60439, USA
[2)]School of Mechanical Engineering, Korea University, Seoul 136-701, Korea

(Received 18 October 2013; Revised 13 November 2013; Accepted 3 January 2014)

ABSTRACT–This paper presents a review of the characterization of physical properties, morphology, and nanostructure of particulate emissions from internal combustion engines. Because of their convenience and readiness of measurement, various on-line commercial instruments have been used to measure the mass, number, and size distribution of nano-particles from different engines. However, these on-line commercial instruments have inherent limitations in detailed analysis of chemical and physical properties, morphology, and nanostructure of engine soot agglomerates, information that is necessary to understand the soot formation process in engine combustion, soot particle behavior in after-treatment systems, and health impacts of the nano-particles. For these reasons, several measurement techniques used in the carbon research field, i.e., high-resolution transmission electron microscopy (HRTEM), X-ray diffraction (XRD), and Raman spectroscopy, were used for analysis of engine particulate matter (PM). This review covers a brief introduction of several measurement techniques and previous results from engine nano-particle characterization studies using those techniques.

KEY WORDS : Particulate matters (PM), PM characterization, TEM microscopy, X-ray diffraction (XRD), Raman spectroscopy

1. INTRODUCTION

Due to growing concerns with respect to urban air quality and human health, hazardous air pollution (HAPs) from the transportation sector has become a topic of greater interest. Scientific research and medical findings have revealed that ultrafine particles below a size of 100 nm have adverse impacts on human health, and internal combustion engines are the main source of these particles (Dockery *et al.*, 1993; Ostro, 1984; Pope *et al*., 1992). Particles emitted from internal combustion engines are a complex mixture of volatile (organic, sulfate, nitrate fraction) and non-volatile (soot, ash) materials, and the majority consists of carbonaceous soot particles (Myung and Park, 2012). The EU has proposed stringent solid particle mass and number (PN) limits of 4.5 mg/km in the Euro 5b standard of September 2011 and 6.0×10^{11} #/km in the Euro 6c from 2017 for both gasoline and diesel direct-injection passenger vehicles (ECOpoint Inc., 2013).

Engine particulate emissions measured by commercial size-measurement instruments such as SMPS (scanning mobility particle sizer) typically exhibit a bimodal size distribution (Kittelson, 1998). Smaller particles so called the nucleation mode are reported to consist mostly of volatile organics when the contribution of sulfur is negligible (Sakurai *et al*., 2003), whereas the larger particles measured in accumulation mode were found to be soot aggregates. In terms of measurement, the volatile nature of nucleation-mode particles creates difficulties in repeatable measurement because of their size and number dependence on sampling conditions. (Kittelson, 1998; Mathis *et al*., 2004). To reduce the uncertainty of PN measurement, detailed specifications were proposed for sampling and treatment of the exhaust gas in the particle measurement program (PMP) for European particulate regulation (Andersson *et al*., 2007, 2010; Giechaskiel *et al*., 2010). According to this methodology, only solid particles larger than 23 nm are included in the number count, which is defined as the particles that survive after an evaporation tube operated at a temperature of 300–400ºC. In addition to the measurement uncertainties caused by sampling and treatment of exhaust gas, the on-line commercial instruments classify particulate sizes using different equivalent sizes (e.g., mobility diameter, aerodynamic diameter) depending on the measurement principles, which can lead to deviation from the physical dimension of the agglomerate particles (DeCarlo *et al*., 2004). Tandem measurements using two or more on-line instruments have been developed for real-

**Corresponding author.* e-mail: gascar@korea.ac.kr

time measurement of additional nano-particle properties such as density and fractal dimension; however, the accuracy of measurement strongly depends on the assumptions of particle shapes (DeCarlo *et al*., 2004; Park *et al*., 2008).

Because the engine-generated particulates have complex chemical properties with a fractal-like agglomerate structure of carbonaceous primary particles, detailed measurements of chemical composition, physical properties, morphology, and carbon nanostructure are required to understand the fundamentals of the in-cylinder soot formation process and particulate transport, deposition, and oxidation behaviors in after-treatment systems. Researchers have applied various measurement techniques i.e., GC-MS, FT-IR, electron energy-loss spectra (EELS), X-ray absorption near edge spectroscopy (XANES), near-edge X-ray absorption fine structure (NEXAFS), high-resolution transmission electron microscopy (HRTEM), X-ray diffraction (XRD), and Raman spectroscopy, to engine particulate studies for chemical, morphology, nanostructure analyses (Braun *et al*., 2004, 2005; Lee *et al*., 2002, 2003; Maricq, 2007; Song *et al*., 2007; Seong and Boehman, 2013).

In this work, we review characterization studies of the physical properties, morphologies, and nanostructures of engine-generated nano-particles. The measurement principles of several on-line commercial instruments and three representative measurement techniques for carbonaceous nano-particle analysis (HRTEM, XRD, Raman spectroscopy) are briefly introduced, and the morphology and nanostructure changes are surveyed as a function of engine types, operating conditions, and fuel types.

2. SOOT PARTICLE CHARACTERIZATION FROM INTERNAL COMBUSTION ENGINES

Engine soot particles have highly complex chemical and physical properties that can vary depending on engine types, operating conditions, and fuel composition. Soot formation takes place in many stages of the combustion process due to the non-homogeneous nature of the fuel-air mixture, injection duration, and its overlap with the combustion process (Heywood, 1988). As a result, the engine soot particles have different sizes, morphologies, and chemical compositions even in a steady-state operation, which make it difficult to characterize this material. Characterization of engine soot particles can be accomplished in three different ways: (1) chemical characterization of soot, (2) physical and morphological characterization of soot agglomerates, and (3) nanostructure characterization of soot primary particles.

The chemical properties of soot are closely related to health impact via carcinogens such as aldehydes and PAHs (polycyclic aromatic hydrocarbons) as well as the oxidation reactivity of soot particles with surface functional groups (Song *et al*., 2007). Depending on the chemical species different sampling and analysis methods are required to analyze the chemical components adsorbed and condensed in soot particles (Maricq, 2007). Details of the chemical characterization of soot will not be covered in this review.

2.1. Physical and Morphological Characterization of Engine Soot Agglomerates

Various on-line measurement instruments are available for size measurement of submicron engine soot particles.

Each instrument reports a different "equivalent diameter" of submicron particles according to the measurement principle that it uses. For example, DMA (differential mobility analyzer) and SMPS measure the electron mobility diameter (d_m), whereas AMS (aerosol mass spectrometer) measures the vacuum aerodynamic diameter (d_{va}). The electrical mobility diameter is the diameter of a sphere with the same migration velocity in a constant electric field as the particle of interest. The aerodynamic diameter (d_a) is defined as the diameter of a sphere with a standard density that settles at the same terminal velocity as the particle of interest. In the free-molecular regime (where Kn >> 1 and the mean free path of the gas molecules is much longer than the particle radius), the aerodynamic diameter is referred to as the vacuum aerodynamic diameter. By these definitions, d_a increases with increasing particle density, which is different from d_m. Engine soot particles typically have highly irregular shapes, and for irregular particles of unit density, the measured d_a is always smaller than diameter of a volume-equivalent sphere (d_{ve}), whereas the measured d_m is larger than the d_{ve}, as described in Figure 1 (DeCarlo *et al*., 2004).

Both TEM (transmission electron microscopy) and SEM (scanning electron microscopy) have been applied to engine soot particles to observe the detailed size and shape of fractal-like soot agglomerates. Figure 2 shows soot particle images taken by TEM and SEM. Thermophoretic sampling directly from the engine exhaust pipe is one common technique used to sample the engine soot on a TEM grid (Chandler *et al*., 2007; Lapuerta *et al*., 2006, 2007; Lee *et al*., 2002, 2003, 2013; Lee and Zhu, 2004, 2005; Neer and Koylu, 2006; Seong *et al*., 2012; Song and Lee, 2007; Zhu *et al*., 2005). Various sampling methods are available after dilution of exhaust gas, i.e., impactor (Bérubé *et al*., 1999; Chakrabarty *et al*., 2006), low pressure impactor (LPI) (Park *et al*., 2003, 2004a, 2004b; Wentzel *et al*., 2003), filter (Lu *et al*., 2012), and thermophoretic sampling (Soewono and Rogak, 2011). Most recently, soot particles in a diesel spray flame have been directly sampled to better understand the soot formation process (Aizawa *et al*., 2012; Kondo *et a*l., 2011; Kook and Pickett, 2012; Nerva *et al*., 2011).

The primary particle diameter (d_p), radius of gyration (R_g), and fractal dimension (D_f) have been widely used to characterize irregular soot particles based on the mass fractal theory (Mandelbrot, 1983). The value of D_f represents the shape of a fractal-like soot aggregate, whether it is similar to an unlimited straight line ($D_f = 1$) or

to a sphere (D_f = 3). The aggregate growth models report how the particle aggregates form and grow from D_f, as described in Figure 3 (Schaefer, 1988). D_f is described as Equation (1),

$$N = k_f\left(\frac{R_g}{d_p}\right)^{D_f} \quad (1)$$

where N is the number of primary particles per aggregate determined from a 2-D projection image of the soot aggregate using Equation (2), and k_f is a prefactor,

$$N = k_a\left(\frac{A_a}{A_p}\right)^{\alpha} \quad (2)$$

where k_a is a constant of order unity, and α is the ratio between the fractal dimensions of cluster and its projected image (Oh and Sorensen, 1997), and k_a and α are the constants used to account for the effect of primary particle overlap in the two-dimensional TEM images.The fractal dimension of identical soot aggregates can be estimated differently depending on how the particle overlap is treated, e.g., D_f = 1.61 without overlap (α = 1.09, k_a = 1.15, Oh and Sorensen, 1997) and D_f = 1.75 with overlap (α = 1.19, k_a = 1.81, Koylu *et al*., 1995) (Park *et al*., 2004). Lapuerta *et al.* (2006) proposed an iterative method to calculate the correct fractal dimension of a soot aggregate based on the determination of the prefactor of the power law relationship and an overlap parameter as functions of the fractal dimension.

Intensive soot characterization investigations using TEM/SEM microscopy from various engines proved that the engine soot aggregates have morphological similarity, D_f ranges within 1.5–1.9 and d_p ranges within 15–35 nm. The previous results of morphological soot characterization are summarized in Table 1.

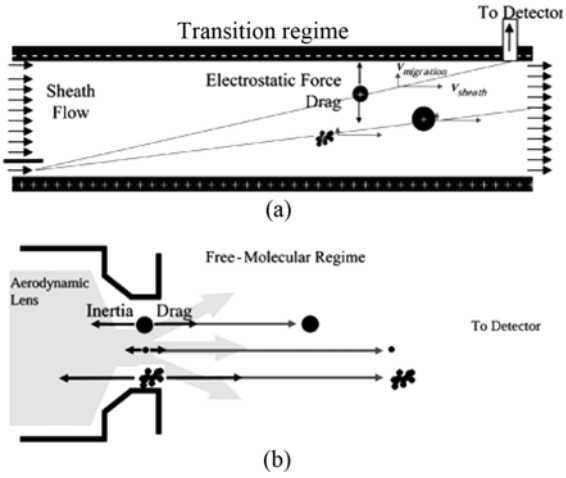

Figure 1. A schematic representation of the different diameter sizing measurements for: (a) DMA (d_m) and (b) AMS (d_{va}). (DeCarlo *et al.*, 2004) [*Reprinted from Aerosol Sci. Technol., 38(12): 1185-1205, 2004, with permission from American Association for Aerosol Research (AAAR)*].

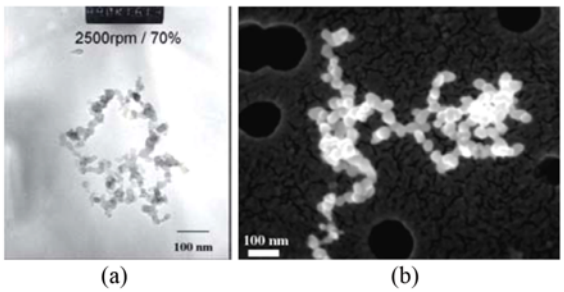

Figure 2. Diesel engine soot particle images taken by: (a) TEM (Lee *et al.*, 2003) and (b) SEM (Gwaze *et al.*, 2006) [*Reprinted from J. aerosol sci., 37(7): 820-838, 2006, with permission from Elsevier*].

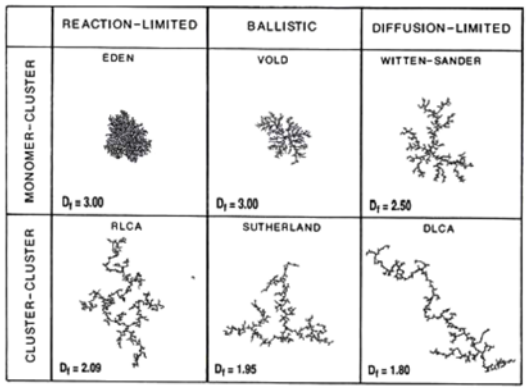

Figure 3. Relationship between agglomerate shape and fractal dimension derived from the aggregate growth models (Schaefer, 1988) [*Reprinted from MRS Bull., 13(2): 22-27, 1998, with permission from Materials Research Society*].

Lee and coworkers performed soot particle characterization for a light-duty diesel engine (Lee *et al*., 2003; Lee and Zhu, 2004, 2005), a heavy-duty diesel engine (Lee *et al*., 2002), a light-duty diesel engine with low temperature combustion (LTC) (Seong *et al*., 2012), and a light-duty DISI gasoline engine (Seong *et al*., 2013). The results showed that the heavy-duty diesel engine tends to produce larger agglomerate and primary particle sizes and a higher fractal dimension than those of the light-duty diesel engine. In advanced combustion modes, i.e., those of LTC and DISI engines, the agglomerate and primary particle sizes become smaller, whereas the fractal dimension is similar to that of the diesel engines. Specifically, a number of aggregates and singlet-like particles less than 20 nm in length were found in the DISI engine, particularly with highly retarded fuel-injection timing (Seong *et al*., 2013). Singlet-like soot particles in the DISI engine with a size of 10–15 nm were also reported by Barone and coworkers (2012).

The effects of engine operating parameters (i.e., air-to-

fuel ratio (A/F), EGR rate, injection, speed and load) and fuel properties on soot morphology have not yet been clearly understood because of insufficient previous data and controversial trends in soot morphology shown in studies. Lapuerta and coworkers (2007) found that the primary particle size is significantly affected by engine speed and A/F and becomes approximately 35% smaller at higher speeds and leaner A/F values. No effects of EGR rate and sampling location on particles were reported in this study, whereas Lee and coworkers reported a larger primary particle size at higher EGR rate (Lee *et al*., 2003) and a decrease in the aggregate primary particle sizes along the exhaust pipe (Lee and Zhu, 2004, 2005). Song and Lee (2007) studied the impacts of fuel properties on diesel particle morphology, and showed that both aromatics and sulfur contents affected particle growth (in size) most significantly, whereas aromatics and naphthene affected the total yield of PM emissions (in mass) most significantly.

Direct TEM sampling from the reacting diesel spray was carried out to gain fundamental insights into the soot formation and oxidation process.

Aizawa and his group sampled soot particles from the spray flame generated in a constant-volume combustion chamber and measured soot particle size and morphology at different axial locations along the spray flame. The results showed that the primary particle size and radius of gyration of soot aggregates increased at 40–50 mm from the nozzle tip, exhibited a peak near 60–70 mm, and decreased downstream of 80–90 mm, locations that correspond to formation, peak concentration, and oxidation of soot particles in the spray, respectively. The fractal dimensions of soot aggregates were found to be constant along the spray, approximately 1.73 (Kondo *et al*., 2011). In a spray flame fueled by soy-methyl ester, the soot particle size reached a peak at 50 mm from the nozzle tip (Nerva *et al*., 2011). The overall morphology of the soy-methyl ester soot bears similarity to that of diesel, but the soot density, primary particle size, and fractal dimension were smaller for biodiesel. (Aizawa *et al*., 2012). Kook and Pickett (2012) obtained TEM soot samples from the spray

Table 1. Previous morphological characterization of engine soot particles via TEM and SEM micrography.

	Engine type	Method	D_f	R_g [μm]	d_p [nm]
Barone *et al*. (2012)	LD DISI gasoline engine 2.0 L, 4-cylinder	TEM	N/A	N/A	20–25 (aggregate) 10–15 (singlet particle)
Chakrabarty *et al*. (2006)	SI engines (3 vehicles) UDC with cold start phase	SEM	1.70–1.78	N/A	N/A
Chandler *et al*. (2007)	MD diesel engine, 5.9 L	TEM	1.80 ± 0.10	0.078–0.135	20–29
Gaddam and Vander wal (2013)	LD DISI gasoline engine Single-cylinder	TEM	1.69–2.37	0.103–0.143	16–25
Lee *et al*. (2002)	HD diesel engine 2.4 L single-cylinder	TEM	1.80–1.88	0.180–0.220	32 ± 3
Lee *et al*. (2003)	LD diesel engine 1.7 L, 4-cylinder	TEM	1.50–1.70	0.077–0.134	22 ± 2 (w/o EGR) 30 ± 5 (with EGR)
Lee and Zhu (2004. 2005)	LD diesel engine 1.7 L, 4-cylinder	TEM	1.46–1.73	0.050–0.102	16–29
Lu *et al*. (2012)	MD diesel engine 4.3 L , 4-cylinder	TEM	N/A	N/A	24–29
Park *et al*. (2004)	MD diesel engine 4.5L, 4-cylinder	TEM	1.75 (with overlapping) 1.61 (w/o overlapping)	N/A	31 ± 7
Seong *et al*. (2012)	LD LTC diesel engine 0.48 L, single-cylinder	TEM	1.57–1.73	0.022–0.031	11–17
Seong *et al*. (2013)	LD DISI gasoline engine 2.4L, 4-cylinder	TEM	1.74–1.81	0.066–0.090	20–29
Soewono and Rogak (2011)	LD diesel engine 1.9 L, 4-cylinder	TEM	1.70–1.85	N/A	N/A
Song and Lee (2007)	LD diesel engine 1.7 L, 4-cylinder	TEM	1.50–1.80	0.035–0.120	20–32
Lapuerta *et al*. (2007)	LD diesel engine 2.2 L 4-cylinder	TEM	N/A	N/A	15–28
Neer and Koylu (2006)	MD diesel engine, 5.9 L	TEM	1.77 ± 0.14	0.160–0.350	20–35
Wentzel *et al*. (2003)	Diesel engine	TEM	1.70 ± 0.13	N/A	22 ± 6

flames of various fuels, i.e., conventional No. 2 diesel (D2), low-aromatics jet fuel (JC), world-average jet fuel (JW), Fischer-Tropsch synthetic fuel (JS), coal-derived fuel (JP), and two-component surrogate fuel (SR), and found that the total soot within the fuel jets decreased in order of D2 = SR > JW > JP > JC > JS, which corresponds to the soot volume fraction trends measured by simultaneous laser extinction measurement and planar laser-induced incandescence imaging.

Tandem measurements using two or more instruments can provide more complete information on such physical properties as mass and density of irregular engine soot particles and enables comparisons of different measures of size, i.e., mobility diameter, optical size, aerodynamic diameter, and volume (Park *et al*., 2008). Measurements with a DMA-LPI were conducted by Skillas and coworkers, and the D_f of soot particles were reported as 2.1 –2.9 for a diesel engine with mobility diameters in the range 55-260 nm (Skilla *et al*., 1998). Maricq and Xu (2004) measured the effective density and D_f from two light-duty diesel vehicles and a direct-injection gasoline vehicle using a DMA-electrical low-pressure impactor (ELPI). The results showed a characteristically steep decrease in the effective density as the particle mobility diameter increases, with values of 1.2 g/cm^3 at 50 nm to 0.3 g/cm^3 at 300 nm, varying weakly with engine types due to the fractal-like nature of soot particles with measured D_f = 2.3 ± 0.1. Virtanen and coworkers (2004) also found similar trend in the particle morphology from a light-duty and a heavy-duty vehicles in which the large particles are less compact, whereas D_f = 2.6–2.8 was reported from mobility diameter and aerodynamic diameter relationships measured by the DMA-ELPI. Park and coworkers used a DMA-aerosol particle mass analyzer (APM) to measure the effective density and D_f of diesel exhaust particles (Part *et al*., 2003), and the particle mass and mobility were related to the structural properties measured by TEM to obtain the dynamic shape factor and the inherent material density (Part *et al*., 2004). Effective densities of 0.3–1.2 g/cm^3 were measured from the mass-mobility relationship at a mobility diameter range of 300–50 nm for various engine conditions. The projected area diameter determined from TEM was equivalent to the mobility diameter, and the differences in the fractal dimensions between the mass-mobility relationship (D_f = 2.35) and TEM (D_f = 1.75) measurements were found to be reasonable in terms of maximum length of soot particle. The mean dynamic shape factor increased from 1.11 to 2.21 and the inherent material density increased from 1.27 g/cm^3 to 1.78 g/cm^3 as the mobility size increased from 50 nm to 220 nm.

2.2. Nanostructure Characterization of Soot Primary Particles

The primary particles of engine soot agglomerates are carbonaceous materials that exhibit a graphitic nanostructure referenced to the size, orientation, and organization of the graphene layers. Compared with well-ordered carbonaceous materials such as graphite, the engine soot can take on wide range of disordered nanostructures depending on the engine types, operating conditions, and fuels. This nanostructure is of interest for particulate filter research because of its relationship to the oxidation reactivity that affects particulate filter regeneration. Raman spectroscopy, XRD, and HRTEM are three main techniques applied for characterization of soot crystalline structure. The crystalline structure of carbonaceous materials contains multiple stacks of individual carbon layers, of which the dimensions are typically defined by the inter-layer spacing (d_{002}), stacking height (L_c), and crystalline basal plane diameter (L_a). The inter-layer spacing of graphite structures has been measured near 0.34 nm if the size of the layers is larger than 2 nm (Belenkov, 2001).

The XRD patterns have been used to derive the d_{002}, L_c, and L_a using well-defined theories such as Bragg's equation and the Scherrer equation (Song *et al*., 2007; Vander wal, 2004; Yehliu *et al*., 2012). Figure 4 shows selected XRD patterns of various soot samples that are clearly distinguished from each other. (Seong and Boehman, 2013).

Raman spectroscopy provides semi-empirical relationships for disordered soot nanostructures in which the first-order Raman spectra shows different characteristic peaks depending on the disorder level of a carbonaceous material. As shown in Figure 5(a), ordered carbonaceous materials such as polycrystalline graphite show two distinct characteristic peaks appearing at ~ 360 cm^1 (D peak) and ~ 1590 cm^1 (G peak), whereas disordered and amorphous carbons also indicate additional peaks appearing at ~ 1180 cm^1 (D4), ~ 1500 cm^1 (D3), and ~1620 cm^1 (D2), which are related to sp^3 carbon or impurities, amorphous carbon, and disordered carbon, respectively (Seong and Boehman, 2013). The Raman spectra are quantified using two different curve-fitting procedures, namely, two-band (Figure 5 (b)) and five-band (Figure 5 (c)) combinations. In the two-band combinations, the ratio of the areas of the D

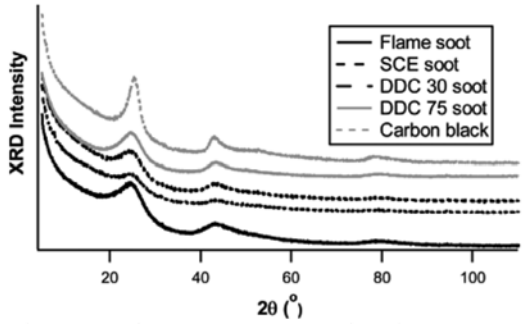

Figure 4. XRD patterns of various soot samples (SCE: single-cylinder diesel engine, DDC: multi-cylinder diesel engine) (Seong and Boehman, 2013) [*Reprinted from Energy Fuels, 27(3): 1613-1624, 2013, with permission from American Chemical Society*].

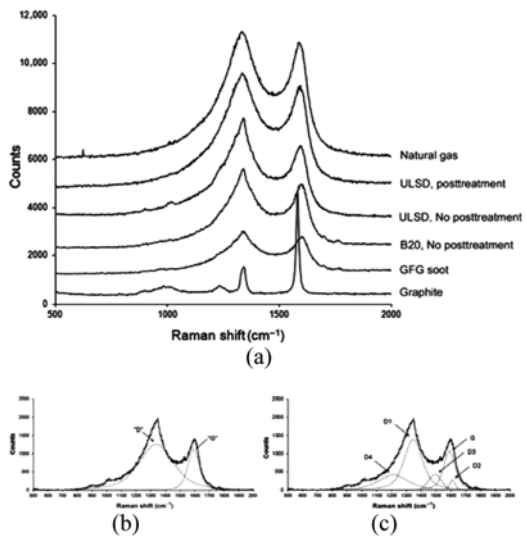

Figure 5. (a) First-order Raman spectra of various samples (vertically offset for clarity), (b) Typical curve fit for Raman spectra using two-band combinations, (c) Typical curve-fit for Raman spectra using five-band combinations (Soewono and Rogak, 2011) [*Reprinted from Aerosol Sci. Technol., 45(10): 1206-1216, 2011, with permission from American Association for Aerosol Research (AAAR)*].

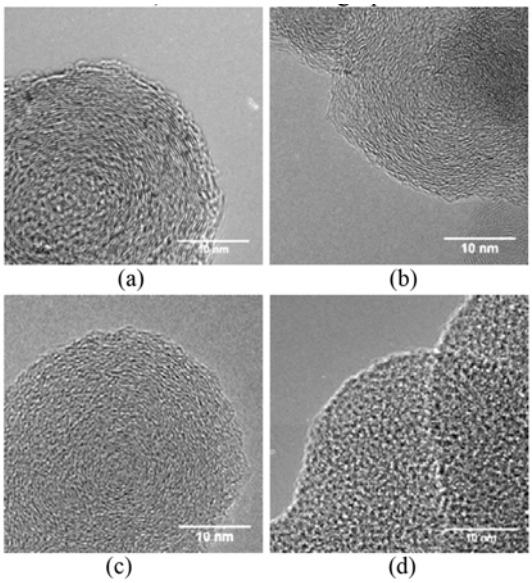

Figure 6. HRTEM images of various soot particles: (a) carbon black, (b) heavy-duty diesel engine, (c) light-duty DISI engine with gasoline, (d) light-duty DISI engine with E85 (Seong *et al.*, 2013) [*Reprinted with permission from SAE paper 2013-01-2574 © 2013 SAE International*].

and G bands (I_D/I_G) serves as an indicator of the disorder of soot. The five-band combinations can be obtained by various curve-fitting methods proposed by Sadezky *et al.* (2005), and the full width at half maximum (FWHM) of the D1 band (the width of D1 band) increases as the graphitic structure order in the soot decreases (Soewono and Rogak, 2011).

The HRTEM has been applied to engine soot particles to visualize the graphitic nanostructure of the primary particles. Although both XRD and Raman spectroscopy measure the crystalline parameters as bulk sample properties, HRTEM can provide the detailed shape of the nanostructure of each individual particle. The order of the nanostructure can be analyzed either qualitatively, by comparing the disordered soot particles (Lu *et al*., 2012; Seong, *et al*., 2013; Song *et al*., 2007; Song and Lee, 2007; Wentzel *et al*., 2003), or quantitatively, by obtaining such crystalline parameters as fringe length, tortuosity, and fringe separation from the image post-processing and statistical analysis (Gaddam and Vander Wal, 2013; Vander Wal *et al*., 2007; Yehliu *et al*., 2012, 2013). Vander wal and his group introduced details of an HRTEM image analysis method for carbon nanostructure quantification (Vander wal *et al*., 2004; Vander wal, 2005; Yehliu *et al*., 2011). Figure 6 shows selected HRTEM images of soot particles with different orders of nanostructures. Well-ordered carbon particles are characterized by smooth concentric fringe patterns surrounding the nucleus and a short interlayer distance between fringe layers, as indicated in (a) carbon black. The primary particles of (b) a heavy-duty diesel and (c) a light-duty DISI engine with gasoline show characteristics of less-ordered structures than carbon black. Soot derived from (d) a light-duty DISI engine with E85 shows an entirely amorphous structure for whole primary particles (Seong *et al*., 2013).

The relationships among engine/fuel conditions, soot nanostructure, and soot reactivity still remain a controversial issue. The effects of diesel engine operation conditions on the nanostructure and reactivity of soot particles were studied by Lu *et al*. (2012) and Yehliu *et al*. (2013). Lu *et al*. (2012) found that soot particles are more ordered (fringe length and tortuosity increase and separation distance decreases) with increasing engine load (decrease of air/fuel ratio), whereas the effect of engine speed is minor. However, Yehliu *et al*. (2013) showed that the impact of engine speed at constant torque is more pronounced than the impact of engine torque (equivalence ratio) at constant engine speed. For the effects of fuel formulation on soot nanostructure and reactivity, Song *et al.* (2007) concluded that there is no definitive impact of the initial nanostructure on the soot oxidation rate, and the relative amount of initial oxygen groups is the more important factor that governs the oxidation rate of diesel particulates. However, recent works by Yehliu *et al*. (2013) demonstrated the opposite results, that the soot oxidative reactivity is dominated by the disorder of the carbonaceous nanostructure and not by the abundance of surface oxygen content.

Analyses on soot particles collected from diesel

particulate filters (DPF) revealed that thermal aging changes the soot particle nanostructures, specifically the "hollow" interior and highly crystalline (ordered) outer shell (Fang and Lance, 2004; Vander wal *et al*., 2007).

Recently, observations of DISI engine soot particles revealed that the DISI engine soot particles are less ordered than typical diesel particulates (Seong *et al*., 2013), and soot particles become less ordered under rich and late end-of-injection conditions, showing higher fringe tortuosity and shorter fringe length (Gaddam and Vander Wal, 2013).

3. CONCLUSION

Stricter regulations on PM have encouraged automakers to develop new engine and after-treatment technologies, and the demands for detailed nano-particle analysis have been increased in an effort understand the nature of engine nano-particles.

Engine soot particles are fractal-like agglomerates of a number of primary particles, and their morphology can be characterized using fractal dimension, radius of gyration, and primary particle diameter. It has been found that the engine nano-particles typically have fractal dimensions of 1.5−1.8 and primary particle diameters of 15−30 nm. Because of the irregular shape of engine nano-particles, the particle diameter is measured differently depending on such measurement principles as mobility diameter and aerodynamic diameter, and understanding the deviation of each diameter from physical dimension is important.

Modern combustion strategies such as DISI and LTC tend to decrease both the agglomerate and primary particle sizes, and singlet-like carbonaceous particles of 10−30 nm in diameter are frequently found. With respect to the nanostructure, modern engines tend to produce particles that are less-ordered than those of model soot and conventional diesel engines. Alternative fuels such as alcohol-blended fuel for SI engines and bio-fuels for diesel engines tend to decrease the order of the nanostructure.

The correlations among in-cylinder combustion/engine operating conditions, soot particle characteristics, and soot oxidation reactivity are important issues; however, it would be premature to offer conclusions for the correlations because previous studies have showed controversial results.

ACKNOWLEDGEMENT–This study was supported by Korea University Grant and BK21 plus.

REFERENCES

Aizawa, T., Nishigai, H., Kondo, K., Yamaguchi, T. Nerva, J., Genzale, C., Kook, S., Pickett, L. M. (2012). Transmission electron microscopy of soot particles directly sampled in diesel spray flame - A comparison between US#2 and biodiesel soot. *SAE Int. J. Fuels Lubr.* **5**, **2**, 665−673.

Andersson, J., Giechaskiel, B., Munoz-Bueno, R., Sandbach, E., Dilara, P. (2007). Particle Measurement Programme (PMP) Light-duty Inter-laboratory Correlation Exercise (ILCE-LD) final report. Institute for Environment and Sustainability. EUR 22775 EN.

Andersson, J., Mamakos, A., Giechaskiel, B., Carriero, M., Martini, G. (2010). Particle Measurement Programme (PMP) Heavy-duty Inter-laboratory Correlation Exercise (ILCE-HD) Final Report. Joint Research Center, Ispra (VA). EUR 24561 EN.

Barone, T. L., Storey, J. M., Youngquist, A. D. and Szybist, J. P. (2012). An analysis of direct-injection spark-ignition (DISI) soot morphology. *Atmos*. *Environ*., **49**, 268−274.

Belenkov, E. A. (2001). Formation of graphite structure in carbon crystallites. *Inorganic Materials* **37**, **9**, 928−934.

Bérubé, K. A., Jones, T. P., Williamson, B. J., Winters, C., Morgan, A. J. and Richards, R. J. (1999). Physicochemical characterisation of diesel exhaust particles: Factors for assessing biological activity. *Atmos*. *Environ*. **33**, **10**, 1599−1614.

Braun, A., Shah, N., Huggins, F. E., Huffman, G. P., Wiricj, S., Jacobsen, C., Kelly, K. and Sarofim, A. F. (2004). A study of diesel PM with X-ray microspectroscopy. *Fuel* **83**, **7**, 997−1000.

Braun, A., Huggins, F. E., Shah, N., Chen, Y., Wirick, S., Mun, S. B., Jacobsen, C. and Huffman, G. P. (2005). Advantages of soft X-ray absorption over TEM-EELS for solid carbon studies – A comparative study on diesel soot with EELS and NEXAFS.. *Carbon* **43**, **1**, 117−124.

Chakrabarty, R. K., Moosmüller, H., Arnott, W. P., Garro, M. A. and Walker, J. (2006). Structural and fractal properties of particles emitted from spark ignition engines. *Environmental Science & Technology* **40**, **21**, 6647−6654.

Chandler, M. F., Teng, Y. and Koylu, U. O. (2007). Diesel engine particulate emissions: A comparison of mobility and microscopy size measurements. *Proc. Combustion Institute* **31**, **2**, 2971−2979.

DeCarlo, P. F., Slowik, J. G., Worsnop, D. R., Davidovits, P. and Jimenez, J. L. (2004). Particle morphology and density characterization by combined mobility and aerodynamic diameter measurements. Part 1: Theory. *Aerosol Science and Technology* **38**, **12**, 1185−1205.

Dockery, D., Pope, C. and Wu, X. (1993). An association between air pollution and mortality in six US cities. *New England J. Med.* **329**, **24**, 1753−1759.

ECOpoint Inc. (2013). http://www.dieselnet.com/ standards/ eu/ld.php

Fang, H. L. and Lance, M. J. (2004). Influence of soot surface changes on DPF regeneration. *SAE Trans*. **113**, **4**, 2053−2061.

Gaddam, C. K. and Vander Wal, R. L. (2012). Physical & chemical characterization of SIDI engine particulates. *Combustion and Flame*, **160**, 2517−2528.

Giechaskiel, B., Chirico, R., DeCarlo, P. F., Clairotte, M.,

Adam, T., Martini, G., Heringa, M. F., Richter, R., Prevot, A. S. H., Baltensperger, U. and Astorga, C. (2010). Evaluation of the Particle Measurement Programme (PMP) protocol to remove the vehicles' exhaust aerosol volatile phase. *Science of the Total Environment* **408**, **21**, 5106–5116.

Gwaze, P., Schmid, O., Annegarn, H. J., Andreae, M. O., Huth, J. and Helas, G. (2006). Comparison of three methods of fractal analysis applied to soot aggregates from wood combustion. *J. Aerosol Science* **37**, **7**, 820–838.

Heywood, J. B. (1988). *Internal Combustion Engine Fundamentals.* McGraw-Hill Book Company. New York.

Kittelson, D. B. (1998). Engines and nanoparticles: A review. *J. Aerosol Sci*., **29**, **5**, 575–588.

Kondo, K., Yamaguchi, T., Nishigai, H., Takano, S. and Aizawa, T. (2011). High-resolution transmission electron microscopy of soot directly sampled at different axial locations in diesel spray flame. *SAE Paper No*. 2011-24-0068.

Kook, S. and Pickett, L. M. (2012). Soot volume fraction and morphology of conventional, fischer-tropsch, coal-derived, and surrogate fuel at diesel conditions. *SAE Int. J. Fuels Lubr.* **5**, **2**, 647–664.

Köylü, Ü. Ö., Faeth, G. M., Farias, T. L. and Carvalho, M. G. (1995). Fractal and projected structure properties of soot aggregates. *Combustion and Flame* **100**, **4**, 621–633.

Lapuerta, M., Ballesteros, R. and Martos, F. J. (2006). A method to determine the fractal dimension of diesel soot agglomerates. *J. Colloid and Interface Science* **303**, **1**, 149–158.

Lapuerta, M., Martos, F. J. and Herreros, J. M. (2007). Effect of engine operating conditions on the size of primary particles composing diesel soot agglomerates. *J. Aerosol Sci*. **38**, **4**, 455–466.

Lee, K. O., Cole, R., Sekar, R., Choi, M. Y., Kang, J. S., Bae, C. S. and Shin, H. D. (2002). Morphological investigation of the microstructure, dimensions, and fractal geometry of diesel particulates. *Proc. Combustion Institute* **29**, **1**, 647–653.

Lee, K., Zhu, J., Ciatti, S., Yozgatligil, A. and Choi, M. Y. (2003). Sizes, graphitic structures and fractal geometry of light-duty eiesel engine particulates. *SAE Paper No*. 2003-01-3169.

Lee, K. O. and Zhu, J. (2004). Evolution in size and morphology of diesel particulates along the exhaust system. *SAE Trans*. **113**, **4**, 1332–1338.

Lee, K. O. and Zhu, J. (2005). Effects of exhaust system components on particulate morphology in a light-duty diesel engine. *SAE Trans*. **114**, **4**, 52–60.

Lee, K., Seong, H., Sakai, S., Hageman, M. and Rothamer, D. (2013). Detailed morphological properties of nanoparticles from gasoline direct injection engine combustion of ethanol blends. *SAE Paper No*. 2013-24-0185.

Lu, T., Cheung, C. S. and Huang, Z. (2012). Effects of engine operating conditions on the size and nanostructure of diesel particles. *J. Aerosol Sci*., **47**, 27–38.

Mandelbrot, B. B. (1983). *The Fractal Geometry of Nature.* Macmillan.

Maricq, M. M. and Xu, N. (2004). The effective density and fractal dimension of soot particles from premixed flames and motor vehicle exhaust. *J. Aerosol Sci*. **35**, **10**, 1251–1274.

Maricq, M. M. (2007). Chemical characterization of particulate emissions from diesel engines: A review. *J. Aerosol Sci*. **38**, **11**, 1079–1118.

Mathis, U., Ristimäki, J., Mohr, M., Keskinen, J., Ntziachristos, L., Samaras, Z. and Mikkanen, P. (2004). Sampling conditions for the measurement of nucleation mode particles in the exhaust of a diesel vehicle. *Aerosol Science and Technology* **38**, **12**, 1149–1160.

Myung, C. L. and Park, S. (2012). Exhaust nanoparticle emissions from internal combustion engines: A review. *Int. J. of Automotive Technology* **13**, **1**, 9–22.

Neer, A. and Koylu, U. O. (2006). Effect of operating conditions on the size, morphology, and concentration of submicrometer particulates emitted from a diesel engine. *Combustion and Flame* **146**, **1**, 142–154.

Nerva, J., Yamaguchi, T., Iguma, H., Nishigai, H., Kondo, K., Takano, S., Aizawa, T., Genzale, C. L. and Pickett, L. M. (2011). Transmission electron microscopy of soot particles sampled directly from a biodiesel spray flame. *SAE Paper No*. 2011-01-2046.

Oh, C. and Sorensen, C. M. (1997). The effect of overlap between monomers on the determination of fractal cluster morphology. *J. Colloid and Interface Science* **193**, **1**, 17–25.

Ostro, B. (1984). A research for a threshold in the relationship of air pollution to mortality: A reanalysis of London winters. *Environ. Health Perspect.*, **58**, 397–399.

Park, K., Cao, F., Kittelson, D. B. and McMurry, P. H. (2003). Relationship between particle mass and mobility for diesel exhaust particles. *Environmental Science & Technology* **37**, **3**, 577–583.

Park, K., Kittelson, D. B., Zachariah, M. R. and McMurry, P. H. (2004a). Measurement of inherent material density of nanoparticle agglomerates. *J. Nanoparticle Research* **6**, **2**, 267–272.

Park, K., Kittelson, D. B. and McMurry, P. H. (2004b). Structural properties of diesel exhaust particles measured by transmission electron microscopy (TEM): Relationships to particle mass and mobility. *Aerosol Science and Technology* **38**, **9**, 881–889.

Park, K., Dutcher, D., Emery, M., Pagels, J., Sakurai, H., Scheckman, J. and McMurry, P. H. (2008). Tandem measurements of aerosol properties — A review of mobility techniques with extensions. *Aerosol Science*

and Technology **42**, **10**, 801–816.

Pope, C., Schwartz, J. and Ransom, M. (1992). Daily mortality and PM10 pollution in utah valley. *Arch. Environ. Health* **47**, **3**, 211–217.

Sadezky, A., Muckenhuber, H., Grothe, H., Niessner, R. and Pöschl, U. (2005). Raman microspectroscopy of soot and related carbonaceous materials: Spectral analysis and structural information. *Carbon* **43**, **8**, 1731–1742.

Sakurai, H., Tobias, H. J., Park, K., Zarling, D., Docherty, K. S., Kittelson, D. B., McMurry, P. H. and Ziemann, P. J. (2003). On-line measurements of diesel nanoparticle composition and volatility. *Atmos. Environ.* **37**, **9**, 1199–1210.

Schaefer, D. W. (1988). Fractal models and the structure of materials. *MRS Bull* **13**, **2**, 22–27.

Seong, H., Lee, K., Choi, S., Adams, C. and Foster, D. (2012). Characterization of particulate morphology, nanostructures, and sizes in low-temperature combustion with biofuels. *SAE Paper No*. 2012-01-0441.

Seong, H. J. and Boehman, A. L. (2013). Evaluation of raman parameters using visible raman microscopy for soot oxidative reactivity. *Energy & Fuels* **27**, **3**, 1613–1624.

Seong, H., Lee, K. and Choi, S. (2013). Effects of engine operating parameters on morphology of particulates from a gasoline direct injection (GDI) engine. *SAE Paper No*. 2013-01-2574.

Skillas, G., Künzel, S., Burtscher, H., Baltensperger, U. and Siegmann, K. (1998). High fractal-like dimension of diesel soot agglomerates. *J. Aerosol Sci*. **29**, **4**, 411–419.

Soewono, A. and Rogak, S. (2011). Morphology and raman spectra of engine-emitted particulates. *Aerosol Science and Technology* **45**, **10**, 1206–1216.

Song, J., Alam, M. and Boehman, A. L. (2007). Impact of alternative fuels on soot properties and DPF regeneration. *Combustion Science and Technology* **179**, **9**, 1991–2037.

Song, J. and Lee, K. O. (2007). Fuel property impacts on diesel particulate morphology, nanostructures, and NOx emissions. *SAE Paper No*. 2007-01-0129.

Vander Wal, R. L., Tomasek, A. J., Pamphlet, M. I., Taylor, C. D. and Thompson, W. K. (2004). Analysis of HRTEM images for carbon nanostructure quantification. *J. Nanoparticle Research* **6**, **6**, 555–568.

Vander Wal, R. L. (2005). Soot nanostructure: Definition, quantification and implications. *SAE Trans*. **114**, **4**, 429–436.

Vander Wal, R. L., Yezerets, A., Currier, N. W., Kim, D. H. and Wang, C. M. (2007). HRTEM study of diesel soot collected from diesel particulate filters. *Carbon* **45**, **1**, 70–77.

Virtanen, A. K., Ristimäki, J. M., Vaaraslahti, K. M. and Keskinen, J. (2004). Effect of engine load on diesel soot particles. *Environmental Science & Technology* **38**, **9**, 2551–2556.

Wentzel, M., Gorzawski, H., Naumann, K. H., Saathoff, H. and Weinbruch, S. (2003). Transmission electron microscopical and aerosol dynamical characterization of soot aerosols. *J. Aerosol Sci*. **34**, **10**, 1347–1370.

Yehliu, K., Vander Wal, R. L. and Boehman, A. L. (2011). Development of an HRTEM image analysis method to quantify carbon nanostructure. *Combustion and Flame* **158**, **9**, 1837–1851.

Yehliu, K., Vander Wal, R. L., Armas, O. and Boehman, A. L. (2012). Impact of fuel formulation on the nanostructure and reactivity of diesel soot. *Combustion and Flame*, **159**, 3597–3606.

Yehliu, K., Armas, O., Vander Wal, R. L. and Boehman, A. L. (2013). Impact of engine operating modes and combustion phasing on the reactivity of diesel soot. *Combustion and Flame*, **160**, 682–691.

Zhu, J., Lee, K. O., Yozgatligil, A. and Choi, M. Y. (2005). Effects of engine operating conditions on morphology, microstructure, and fractal geometry of light-duty diesel engine particulates. *Proc. Combustion Institute* **30**, **2**, 2781–2789.